

Article

Are GRMHD Mean-Field Dynamo Models of Thick Accretion Disks SANE?

Niccolò Tomei ^{1,2,3,*} , Luca Del Zanna ^{1,2,3} , Matteo Bugli ⁴  and Niccolò Bucciantini ^{1,2,3} 

- ¹ Dipartimento di Fisica e Astronomia, Università degli Studi di Firenze, Via G. Sansone 1, I-50019 Sesto Fiorentino, Italy; luca.delzanna@unifi.it (L.D.Z.); niccolo.bucciantini@inaf.it (N.B.)
- ² INAF, Osservatorio Astrofisico di Arcetri, Largo E. Fermi 5, I-50125 Firenze, Italy
- ³ INFN, Sezione di Firenze, Via G. Sansone 1, I-50019 Sesto Fiorentino, Italy
- ⁴ Département d’Astrophysique, CEA—Saclay, Orme des Merisiers, F-91191 Gif-sur-Yvette, France; matteo.bugli@cea.fr
- * Correspondence: niccolo.tomei@unifi.it

Abstract: The remarkable results by the Event Horizon Telescope collaboration concerning the emission from M87* and, more recently, its polarization properties, require an increasingly accurate modeling of the plasma flows around the accreting black hole. Radiatively inefficient sources such as M87* and Sgr A* are typically modeled with the SANE (standard and normal evolution) paradigm, if the accretion dynamics is smooth, or with the MAD (magnetically arrested disk) paradigm, if the black hole’s magnetosphere reacts by halting the accretion sporadically, resulting in a highly dynamical process. While the recent polarization studies seem to favor MAD models, this may not be true for all sources, and SANE accretion surely still deserves attention. In this work, we investigate the possibility of reaching the typical degree of magnetization and other accretion properties expected for SANE disks by resorting to the mean-field dynamo process in axisymmetric GRMHD simulations, which are supposed to mimic the amplifying action of an unresolved magnetorotational instability-driven turbulence. We show that it is possible to reproduce the main diagnostics present in the literature by starting from very unfavorable initial configurations, such as a purely toroidal magnetic field with negligible magnetization.

Keywords: accretion disks; relativistic processes; magnetohydrodynamics (MHD); dynamo



Citation: Tomei, N.; Del Zanna, L.; Bugli, M.; Bucciantini, N. Are GRMHD Mean-Field Dynamo Models of Thick Accretion Disks SANE? *Universe* **2021**, *7*, 259. <https://doi.org/10.3390/universe7080259>

Academic Editor: Lorenzo Iorio

Received: 22 June 2021
Accepted: 21 July 2021
Published: 23 July 2021

Publisher’s Note: MDPI stays neutral with regard to jurisdictional claims in published maps and institutional affiliations.



Copyright: © 2021 by the authors. Licensee MDPI, Basel, Switzerland. This article is an open access article distributed under the terms and conditions of the Creative Commons Attribution (CC BY) license (<https://creativecommons.org/licenses/by/4.0/>).

1. Introduction

A current challenge in astrophysics is the accurate modeling of the accretion of magnetized plasma onto supermassive black holes. The surprising observational results by the EHT (Event Horizon Telescope) project have opened the possibility to directly test sophisticated theoretical models, typically general relativistic magnetohydrodynamical (GRMHD) numerical simulations, against observations. The asymmetric ring image of the M87 galaxy’s compact radio source was reproduced by ray tracing codes in the curved spacetime of the black hole region, using the emission properties of the extremely hot plasma arising from GRMHD simulations [1]. The further processing of polarized emission on the event horizon scale has allowed an even more accurate estimation of the fundamental physical properties of the accreting plasma, such as density, magnetic field intensity, and electron temperature [2].

The study of the polarization properties of M87* radio emission has also allowed for considerable progress in the choice of the correct modeling paradigm for the accretion dynamics. It is known that for RIAF (radiatively inefficient accretion flow [3–6]) sources such as M87* and even SgrA*, the horizon-penetrating (normalized) magnetic flux ϕ can at most increase up to a maximum threshold ϕ_{\max} , which depends on the spin of the black hole and the scale height of the disk [7]. If $\phi \sim \phi_{\max}$, the black hole is unable to continuously absorb the whole magnetic field, since the accumulation of such a field in

its magnetosphere significantly affects the dynamics of the accretion, leading to sporadic major accretion events and to discontinuous motion of the cusp of the accreting disk. This regime is known as MAD (magnetically arrested disk [8,9]), as opposed to the SANE (standard and normal evolution, [10,11]), where $\phi < \phi_{\max}$, and the accretion is basically unaffected by the black hole magnetosphere. The comparison with the polarized image made it possible to select a subset of MAD models from the GRMHD simulation libraries compatible with observations.

Although SANE models now seem to be less favored compared to MAD models for M87*, they can still be considered an interesting case for other sources and a perfect benchmark for GRMHD theoretical models. Recently, the Code Comparison Project by Porth and EHT-Collaboration [12] showed the ability of the GRMHD community to produce robust modeling of the accretion in SANE disks: by adopting the same initial conditions and resolution, various state-of-the-art codes employing very different numerical strategies were able to obtain consistent results, demonstrating the maturity reached by GRMHD simulations. In this project, the magnetic field inside the disk was initialized with a poloidal loop with a maximum magnetization, that is, the ratio of magnetic to rest mass energy densities, of $\sigma_{\max} \sim 10^{-2}$, while pressure perturbations were introduced to trigger the magnetorotational instability (MRI, [13,14]), as it is needed to start the accretion process. The output of the various codes was validated by cross-comparing results against a suite of selected diagnostics, which are currently considered a standard benchmark for this kind of simulation.

However, such numerical models assume an initial magnetic field whose intensity is set to a high enough value as to properly resolve the onset of the MRI, rather than matching a physically relevant scenario. We can think of a more agnostic situation in which the initial magnetic field has a simpler morphology and a negligible magnetization; it is then amplified inside the disk by small-scale motions until it reaches the intensity and degree of turbulence necessary to initiate the accretion. Without resorting to computationally expensive 3D global simulations, it is possible to achieve this effect by using the simple mean-field dynamo approach [15–18] even in 2D axisymmetric simulations. This is obtained by introducing in the resistive Ohm's law—a new term proportional to the magnetic field itself—which describes the coupling between the velocity and magnetic field unresolved turbulent fluctuations, with a main effect being the creation of a poloidal magnetic component from a toroidal one (the so-called α effect). At the same time, the differential rotation of the accretion disk deforms the poloidal magnetic field lines, producing a toroidal component (Ω effect), so that the combination of these two effects allows for closing the dynamo cycle and amplifying the magnetic field exponentially (at least in the kinematic phase where the reaction of the plasma is neglected).

In the absence of explicit dynamo terms, this amplification process is expected to naturally take place due to the MRI: both local shearing box simulations [19–21] and global models [22,23] studied the saturation of the MRI in order to characterize the α coefficients; further studies have also considered the effect of the anisotropic nature of the MHD turbulence [24,25]. However, the introduction of explicit dynamo terms allows for regulating the growth of selected field components in different spatial regions of the source, while MRI is more limited by the initial magnetic configuration.

The covariant 3 + 1 formalism for the mean-field dynamo within the context of GRMHD, together with the required specific numerical strategies, was presented by Bucciantini and Del Zanna [26] and Del Zanna and Bucciantini [27]. The first applications to compact objects are due to Bugli et al. [28] and Franceschetti and Del Zanna [29], both in the kinematic regime. The first fully nonlinear study applied to accretion disks around black holes is the work by Tomei et al. [30] (TO20 from here on), where the magnetic field is amplified from negligible magnetizations up to basically reaching equipartition with the plasma, hence sufficient to explain observations (synchrotron emission from Sgr A*). In the first phase, there is the exponential growth of the magnetic field, as already observed

by Bugli et al. [28]. Later the dynamo process naturally quenches, interestingly to a level which is basically independent of the (unknown) dynamo and resistivity coefficients.

The main results of TO20 were recently confirmed by Vourellis and Fendt [31], including the case of a thin accretion disk, generalizing the results of Vourellis et al. [32]. In addition, the mean-field dynamo approach has also been adopted in jet launching simulations [33,34], while the effects of magnetic reconnection have been studied by Ripperda et al. [35].

The goal of the present paper is to extend the analysis of TO20 to a wider range of parameters and to much longer dynamical times and, above all, to reproduce the relevant standard diagnostics of the Code Comparison Project, and hence also the EHT observations, by using axisymmetric GRMHD simulations of accretion disks with mean-field dynamo action. The main purpose is to show how we can correctly model the SANE accretion scenario, even adopting much cheaper 2D simulations, rather than 3D, and this can be achieved by starting from a more agnostic, though very unfavorable, initial configuration of a very weak (toroidal) magnetic field ($\sigma_{\max} \sim 10^{-6}$), which is to be naturally amplified in both the toroidal and poloidal components by the action of the dynamo.

2. Disk Model and Numerical Setup

In our simulations, we considered the hydrodynamic torus described by the Fishbone–Moncrief’s solution [36] commonly adopted in the literature, as well as in Porth and EHT-Collaboration [12]. The space-time is determined by a Kerr black hole with dimensionless spin $a = 0.9375$ (from here on, we use units with $G = c = 1$). The inner edge of the disk is localized at $r_{in} = 6M$, and the density has a maximum of $\rho = \rho_c$ at $r_c = 12M$. We assumed an ideal gas equation of state with adiabatic index $\hat{\gamma} = 4/3$. Unlike TO20, here, we chose to superimpose on the hydrodynamic torus an initial toroidal magnetic field with negligible amplitude, so that the equilibrium is essentially preserved. Such a configuration is the most unfavorable to reproduce the conditions observed in ideal GRMHD models, as they generally assume large-scale poloidal magnetic fields. We take an initial magnetic field intensity $B_\phi \propto \rho$ as in Vourellis and Fendt [31], with a maximum magnetization at the center of the torus of $\sigma_{\max} = 10^{-6}$. The resistivity and dynamo profiles are similar to those in TO20, that is:

$$\eta = \begin{cases} \eta_0 \sqrt{\rho/\rho_c} & \rho \geq \rho_{\text{disk}} \\ 0 & \rho < \rho_{\text{disk}}, \end{cases} \tag{1}$$

$$\xi = \begin{cases} \xi_0(\rho/\rho_c) \cos \theta & \rho \geq \rho_{\text{disk}} \\ 0 & \rho < \rho_{\text{disk}}, \end{cases} \tag{2}$$

where η_0 and ξ_0 are the maximum values of the resistivity and dynamo coefficients at $t = 0$ (note that the density varies both in space and time), and $\rho_{\text{disk}} = 10^{-3}\rho_c$ is the density threshold that defines the boundary between disk and atmosphere. We also define the dynamo numbers as in Vourellis and Fendt [31]:

$$C_\Omega = r \left| \frac{\partial \Omega}{\partial r} \right| \frac{H^2}{\eta}, \tag{3}$$

$$C_\xi = H \frac{\xi}{\eta}, \tag{4}$$

where $\Omega = u^\phi/u^t$, and $H \simeq 0.25r$ is the scale height of the disk.

Using the horizon-penetrating Kerr–Schild coordinates, we carried out a series of axisymmetric simulations, expanding the range of parameters with respect to TO20 (see Table 1). In order to assess the validity of our results with respect to the diagnostics in the Code Comparison Project, we adopted the same resolutions as the simulations of Porth and EHT-Collaboration [12] (see Table 2 for details). Unlike in TO20, here, we did not adopt

any explicit dynamo quenching. All the simulations were carried out using the ECHO code [37], with its most recent improvements described in Bugli [38] and Bugli et al. [39].

Table 1. Maximum initial values of η , ζ , C_Ω , and C_ζ for each model.

Run	η_0	ζ_0	$C_{\Omega,0}^{max}$	$C_{\zeta,0}^{max}$
Eta-3Xi-3	10^{-3}	10^{-3}	8.2×10^4	0.75
Eta-3Xi-2	10^{-3}	10^{-2}	8.2×10^4	7.5
Eta-3Xi-1	10^{-3}	10^{-1}	8.2×10^4	75
Eta-4Xi-3	10^{-4}	10^{-3}	8.2×10^5	7.5
Eta-4Xi-2	10^{-4}	10^{-2}	8.2×10^5	75
Eta-4Xi-1	10^{-4}	10^{-1}	8.2×10^5	750

Table 2. Details on the numerical grid adopted. Here $r_h \simeq M$ is the event horizon radius.

Axis	Grid Points	Domain	Stretching
r	192	$(r_h - 0.25M, 3000M)$	Logarithmic
θ	192	$(0.06, \pi - 0.06)$	Uniform

3. Results

We first describe the time evolution of the radial magnetic field in the torus driven by the mean-field dynamo. The creation of a poloidal component within the disk begins from the earliest times, as shown in Figure 1, where the temporal evolution of the disk-averaged $\langle |b^r| \rangle$, with $|b^r| = \sqrt{b^r b^r g_{rr}}$, is plotted (we consider the comoving field). Here, the averaging operation of any quantity q is defined as in Porth and EHT-Collaboration [12]:

$$\langle q \rangle = \frac{\int_{r_{min}}^{r_{max}} \int_{\theta_{min}}^{\theta_{max}} q \sqrt{-g} \, dr d\theta}{\int_{r_{min}}^{r_{max}} \int_{\theta_{min}}^{\theta_{max}} \sqrt{-g} \, dr d\theta} \tag{5}$$

regardless of q being a scalar quantity or a tensorial component (as in the case we are discussing), where $r_{min} = r_h$, $r_{max} = 50M$, $\theta_{min} = \pi/3$, $\theta_{max} = 2\pi/3$.

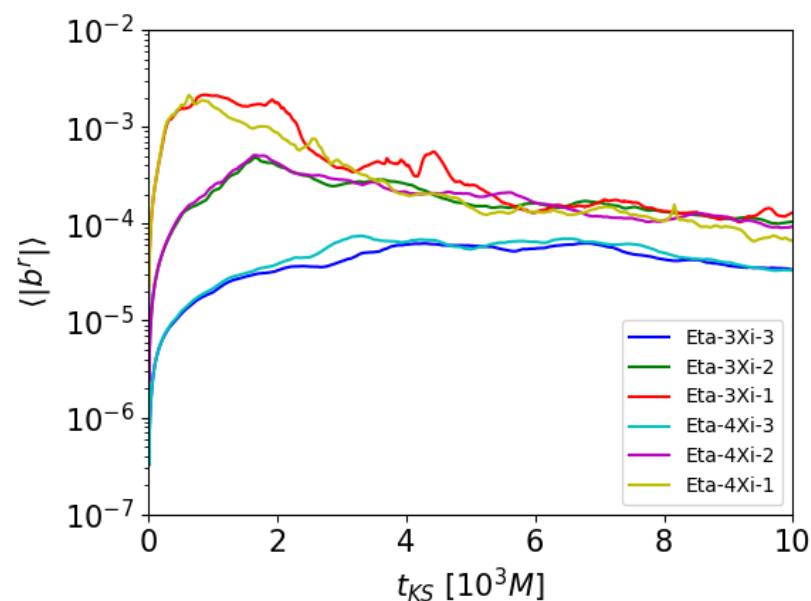


Figure 1. Time evolution of $|b^r|$ averaged on the disk for each model.

The dependence on ζ_0 (i.e., the dynamo α effect) is evident in the duration of the initial kinematic phase, in the steepness of the curve, and in the maximum value that is reached: the higher the ζ_0 , the faster the evolution towards a higher radial magnetic field value. After a transient, there is a saturation phase followed by a decrease in $|b^r|$ inside the torus. In particular, in the runs of strong and intermediate dynamo, the saturation value is similar, while it is lower in models with weak dynamo. As shown later, the low intensity of the initial dynamo in runs Eta-3Xi-3 and Eta-4Xi-3 seems not to be able to produce the turbulence needed to resolve the fastest growing mode of the MRI, and thus, the accretion is entirely driven by the action of the weak dynamo.

The decrease of the amplification of the poloidal magnetic field in all simulations does not seem to depend on an intrinsic decrease in dynamo action. Figure 2 shows that dynamo numbers remain fairly constant over time. The most likely explanation is that the fragmentation of the magnetic structures leads to a global loss of efficiency in the dynamo coupling mechanism, hence leading naturally to a self-regulated quenching, as first observed by TO20 and later confirmed in Vourellis and Fendt [31].

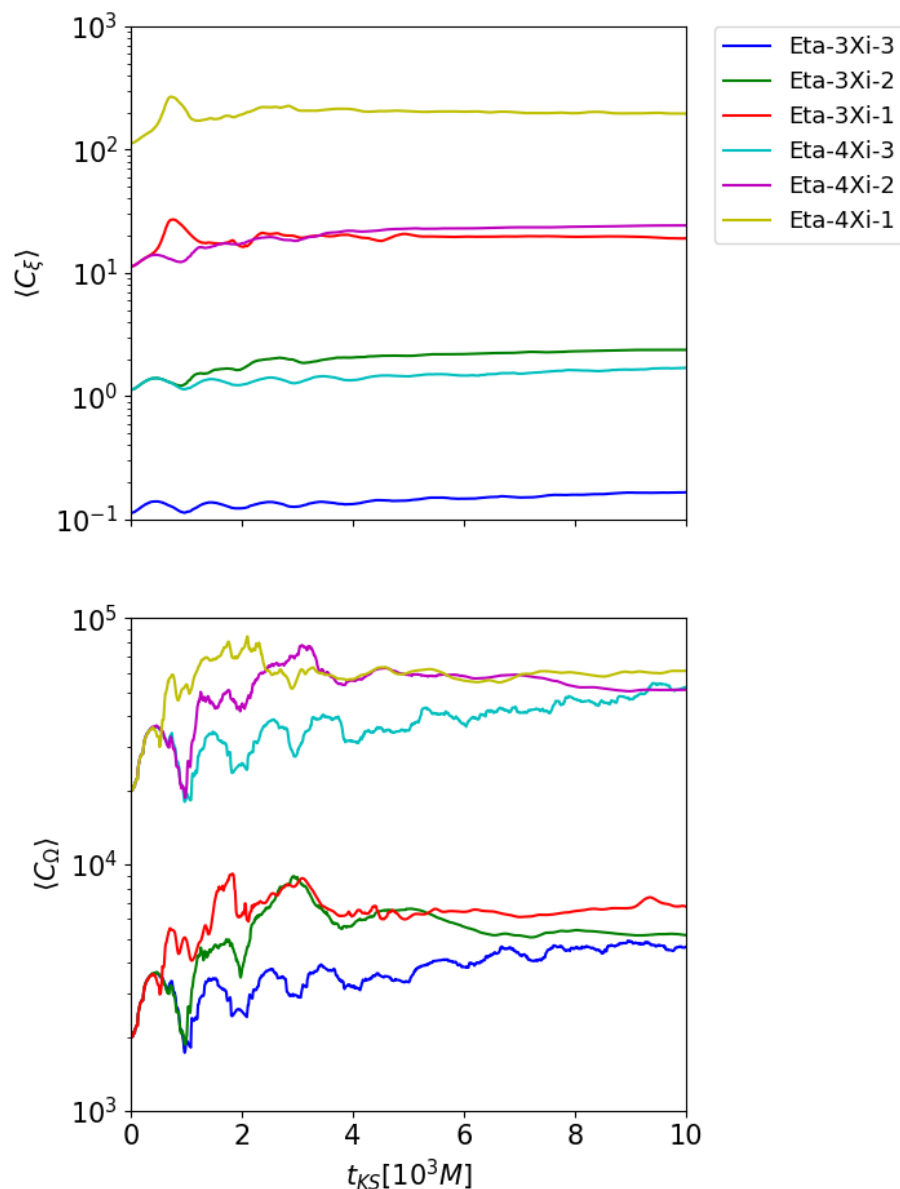


Figure 2. Time evolution of the dynamo numbers averaged on the disk for each model.

In order to understand whether the accretion regime that is established in our dynamo runs is consistent with 3D ideal GRMHD simulations of SANE disks, in the remainder of the paper, we attempt to reproduce the main standard diagnostics as studied in Porth and EHT-Collaboration [12].

3.1. Horizon Penetrating Fluxes

We briefly recall that the definitions of the mass, magnetic, angular momentum and energy fluxes evaluated at the horizon (see Section 5.1 in Porth and EHT-Collaboration [12]) in the axisymmetric case are

$$\dot{M} = 2\pi \int_0^\pi \rho u^r \sqrt{-g} d\theta, \tag{6}$$

$$\Phi_{BH} = \pi \int_0^\pi |{}^*F^{rt}| \sqrt{-g} d\theta, \tag{7}$$

$$\dot{L} = 2\pi \int_0^\pi T_\phi^r \sqrt{-g} d\theta, \tag{8}$$

$$\dot{E} = 2\pi \int_0^\pi (-T_t^r) \sqrt{-g} d\theta, \tag{9}$$

where ${}^*F^{\mu\nu}$ is the Maxwell tensor, and $T^{\mu\nu}$ is the stress-energy tensor. Usually, the fluxes defined by (6)–(9) are normalized with the accretion rate \dot{M} . In particular, the normalized magnetic flux is defined as

$$\phi = \frac{\Phi_{BH}}{\sqrt{\dot{M}}} \tag{10}$$

and it is also known as the MAD parameter, since we can discriminate against the SANE and MAD regimes based on its critical value. In particular, the critical value above which the MAD regime is favored is $\phi = 15$ in the case of a black hole with spin $a = 0.9375$ and a disk with scale ratio $H/R \sim 0.25$ [7].

In the ideal simulations of Porth and EHT-Collaboration [12], the accretion starts at $t \simeq 300M$ when the linear MRI, triggered by pressure perturbations, is captured. After the transient, ϕ reaches the value $\phi \sim 1$, typical of the SANE regime. Accretion rate, angular momentum flow, and net energy flow efficiency also become stationary, with average values of $\dot{M} \sim 0.1$, $\dot{L}/\dot{M} \sim 2$, and $|\dot{E} - \dot{M}|/\dot{M} \sim 0.05$.

Figure 3 shows the time series of the normalized fluxes obtained in our dynamo runs. The evolution clearly depends on the value of ξ_0 , while there is no substantial dependence on η_0 . The two runs with weak dynamo (Eta-3Xi-3, Eta-4Xi-3) produce low accretion rates and cannot be considered good SANE models. Instead, the two runs with intermediate dynamo (Eta-3Xi-2, Eta-4Xi-2) show a very good agreement with the results shown in Figure 4 of Porth and EHT-Collaboration [12]: the accretion starts at $t \sim 1000 M$, and after an initial transient, the accretion rate saturates to the value of $\dot{M} \sim 0.1$.

The magnetic flux and the angular momentum flux remain almost constant during the simulation, $\phi \sim 1$ and $\dot{L}/\dot{M} \sim 2$. The trend in net energy flow efficiency, $(\dot{E} - \dot{M})/\dot{M}$, differs slightly from that of Porth and EHT-Collaboration [12]: in our dynamo models it can assume negative values, although the final value is consistent with the one presented in the code comparison project, $(\dot{E} - \dot{M})/\dot{M} \lesssim 0.1$. Finally, the two models with strong dynamo (Eta-3Xi-1, Eta-4Xi-1) show a good agreement with Porth and EHT-Collaboration [12], although with some differences compared to the case of intermediate dynamo. The initial transient is characterized by a higher and more impulsive accretion rate.

The magnetic flux in our models with $\xi_0 = 0.1$ is on average higher, with run Eta-3Xi-1 even showing two intensity spikes approaching the critical threshold of $\phi = 15$. The action of the stronger dynamo seems to affect the evolution of the angular momentum flux, which is less smooth and has values $\dot{L}/\dot{M} \lesssim 2$ in the stationary phase. As for net energy flow efficiency, an initial phase dominated by negative values is observed, except for the two positive bursts in run Eta-3Xi-1. The negative contribution to the energy efficiency is given

by the enthalpy term [40]. In our simulations, we note that the contribution of enthalpy grows with ξ_0 , meaning that the black hole is accreting more and more thermo-kinetically unbound matter.

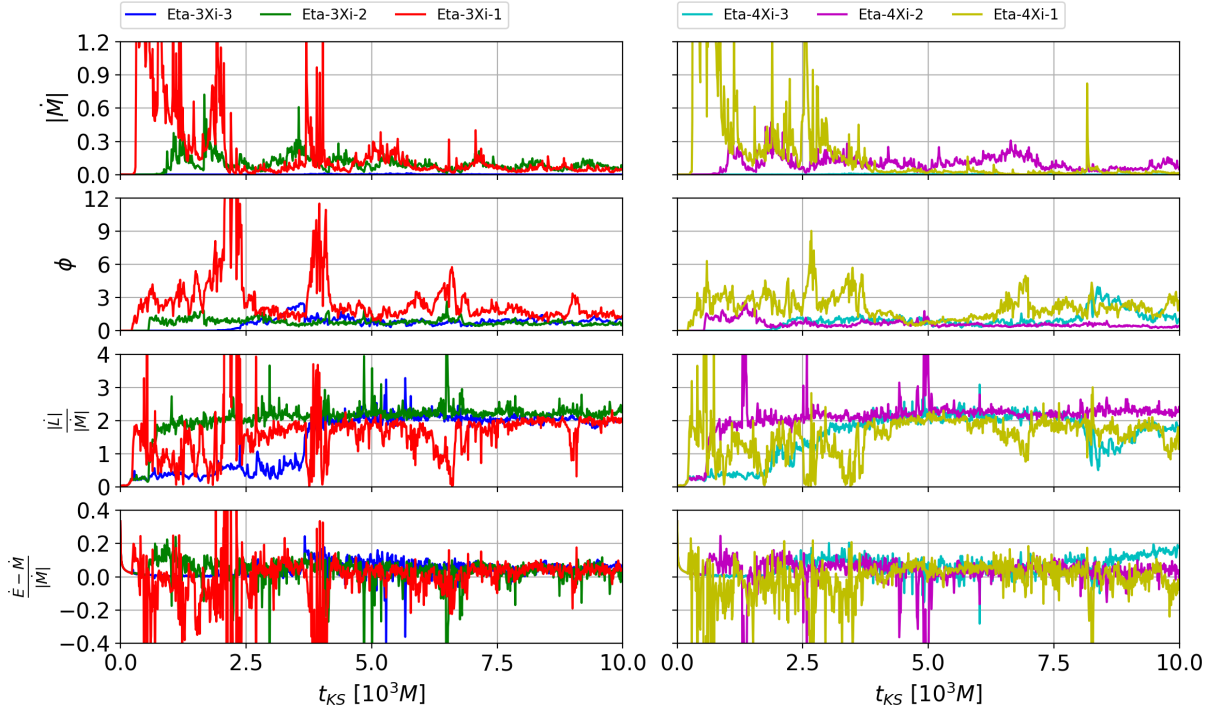


Figure 3. Time series of the horizon penetrating fluxes for each model (on the left panels, runs with $\eta_0 = 10^{-3}$; on the right panels, runs with $\eta_0 = 10^{-4}$).

3.2. MRI Quality Factors

The role of the MRI can be studied from the values assumed by the so-called quality factor. Along the θ direction, it is defined as

$$Q_\theta = \frac{2\pi}{\Omega} \frac{|b^\theta|}{\sqrt{g_{\theta\theta}\Delta\theta} \sqrt{\rho h + b^2}}, \quad (11)$$

where ρh is the enthalpy per unit of volume, Ω the angular velocity of the disk, and $\Delta\theta$ the width of the cell in the θ direction. As in TO20, we considered $\langle Q^\theta \rangle = 6$ to be the threshold for resolving the MRI. Figure 4 shows that there is an initial time interval in which $\langle Q^\theta \rangle > 6$ for runs Eta-3Xi-2, Eta-3Xi-1, Eta-4Xi-2, and Eta-4Xi-1. Then the dissipation stops the MRI and the accretion is driven by the mean-field dynamo. Run Eta-3Xi-1 has a higher value of $\langle Q^\theta \rangle$ and is kept above the threshold for a longer time than the other runs, which is consistent with the higher observed magnetic flux. Overall, according to what has been observed by TO20, it seems that MRI cannot develop for a long time with an axisymmetric mean-field dynamo mechanism: while in the initial transient, MRI and dynamo can coexist, the subsequent stationary phase seems to be regulated exclusively by the self-quenched dynamo.

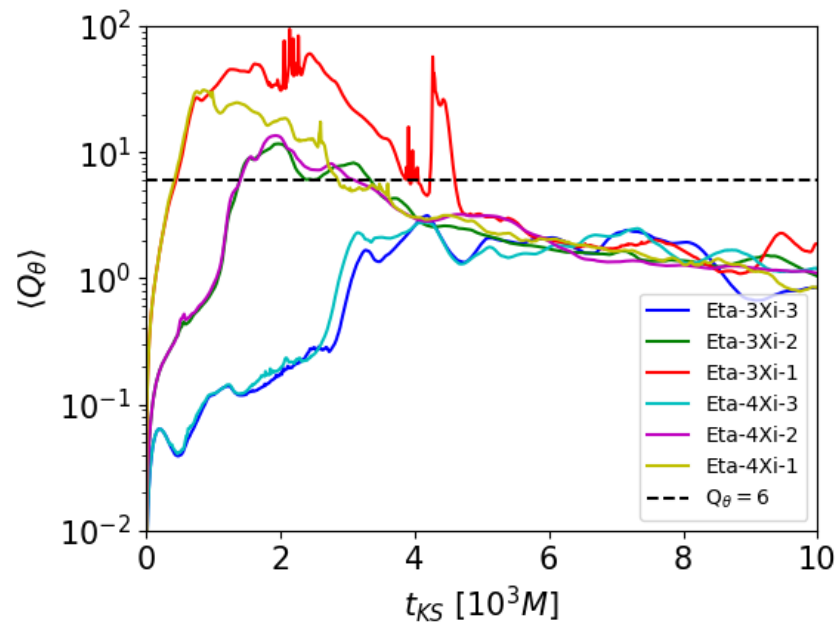


Figure 4. Time evolution of the Q_θ quality factor averaged on the disk for each model. The dashed black line indicates the minimum threshold for solving the linear MRI.

3.3. Time-Averaged Maps

To better appreciate the spatial structure of various quantities, a picture of the quasi-stationary state can be obtained from the time averaged rest-frame density, inverse plasma β , and the magnetization σ (Figures 5 and 6). We identify the disk with the regions occupied by bound denser and weakly magnetized plasma, the funnel by low-density and highly magnetized (Poynting-dominated) plasma, and the jet sheath separating them and containing the larger part of the material outflows. The time window $[5000M, 10,000M]$ is chosen so as to cover the stationary state for all simulations, and by adopting the same color scale used in Porth and EHT-Collaboration [12], we will more easily compare our results.

The dynamo action of the dynamo significantly changes the structure of the torus. By increasing the parameter ζ_0 , the disk evolves to a stationary state with lower density and pressure and has a more flattened shape on the equatorial plane. The funnel and the jet sheath are progressively wider as ζ_0 increases, as the central and right panels in Figures 5 and 6 show. By increasing C_Ω by a factor of 10 (i.e., reducing the resistivity), the contribution of the α effect of the dynamo during the initial transient is probably less dominant, leading the torus to lose less matter and tend more to the ideal case of Porth and EHT-Collaboration [12] (Figure 6).

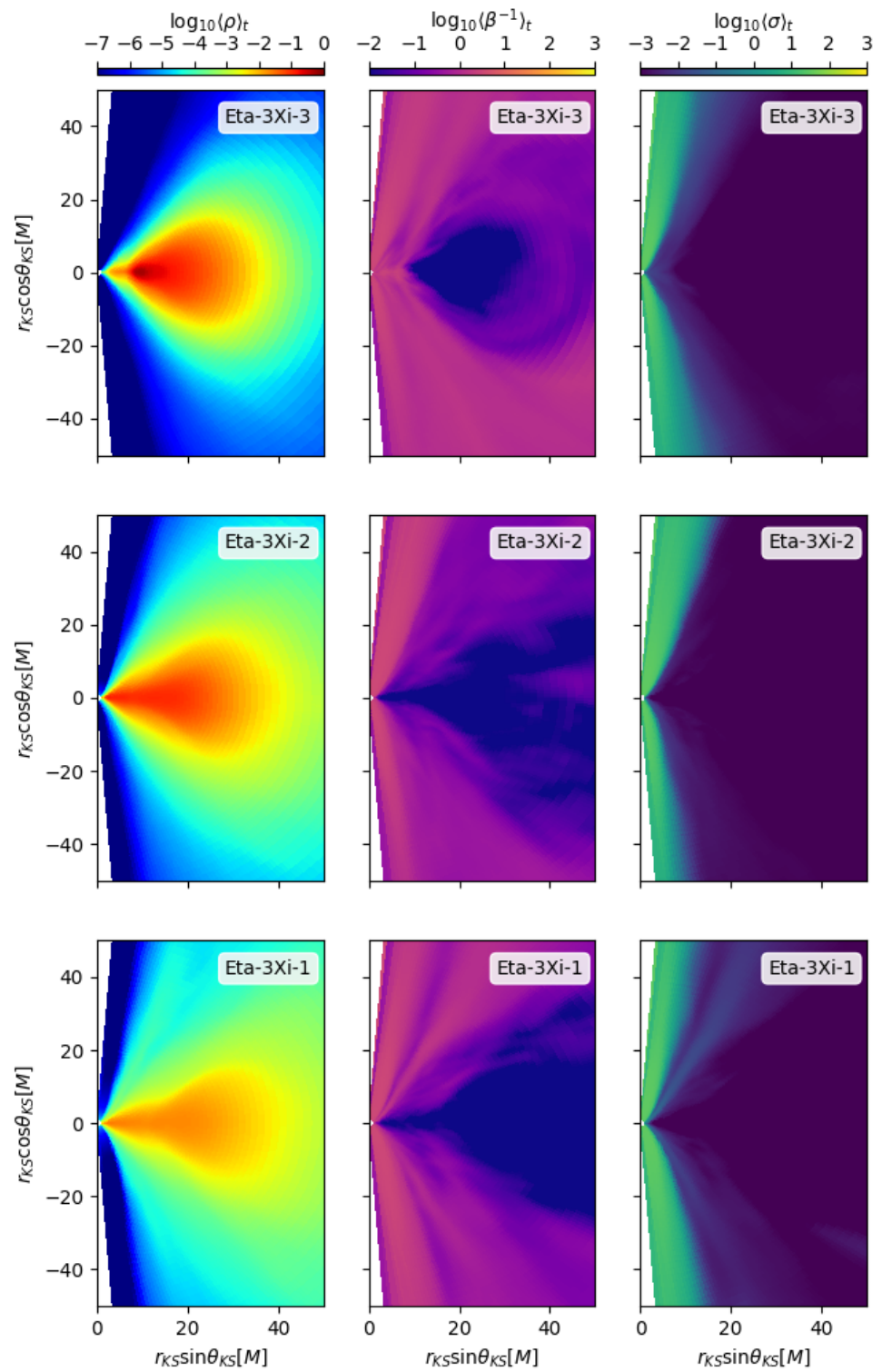


Figure 5. Time-averaged data for rest-mass density, inverse plasma β , and magnetization for runs with $\eta_0 = 10^{-3}$. We indicate with $\langle \cdot \rangle_t$ the time average in the range $[5000M, 10,000M]$.

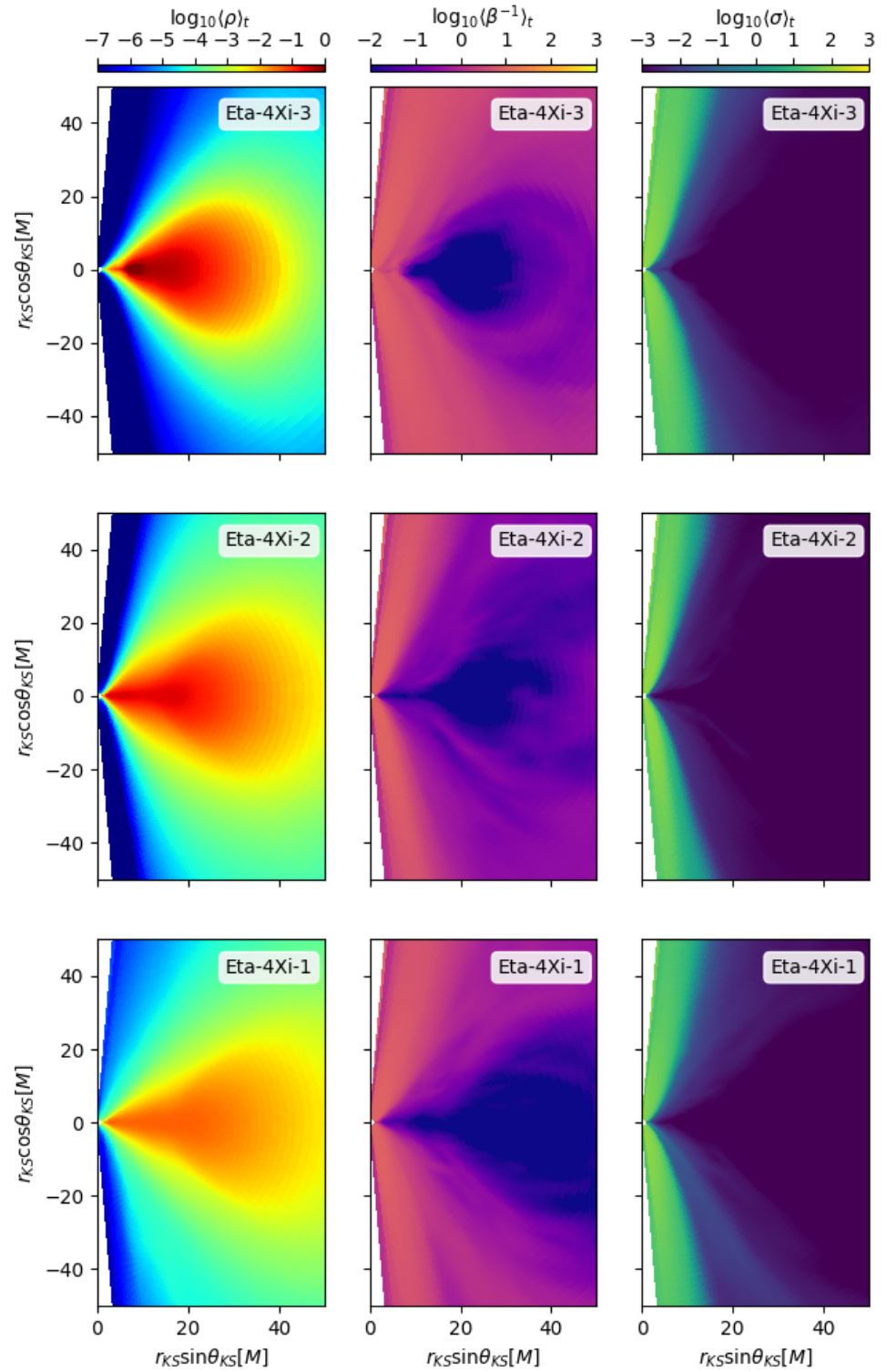


Figure 6. Time-averaged data for rest-mass density, inverse plasma β , and magnetization for runs with $\eta_0 = 10^{-4}$.

3.4. Synchrotron Pseudo-Luminosity

A further diagnostic is a proxy for the luminosity due to (thermal) synchrotron radiation as defined in Porth and EHT-Collaboration [12]:

$$\mathcal{L}(t) = 2\pi \int_{r_{\min}}^{r_{\max}} \int_{\theta_{\min}}^{\theta_{\max}} j(B, p, \rho) \sqrt{-g} d\theta dr \quad (12)$$

where integration boundaries are the same as for disk-averaged quantities, and the pseudo-emissivity is defined as $j(B, p, \rho) = \rho^3 p^{-2} \exp[-C(\rho^2/(Bp^2))^{1/3}]$ with $C = 0.2$ (all quantities in code units). Again, the time series of the luminosity in Figure 7 shows the best agreement with Porth and EHT-Collaboration [12] in the two runs with intermediate dynamo, where $\mathcal{L}/\dot{M} \sim 200$ in the stationary phase. The strong dynamo produces lower luminosity because the disk has lost more matter, while the weak dynamo fails to produce a magnetic field intense enough to support this emission.

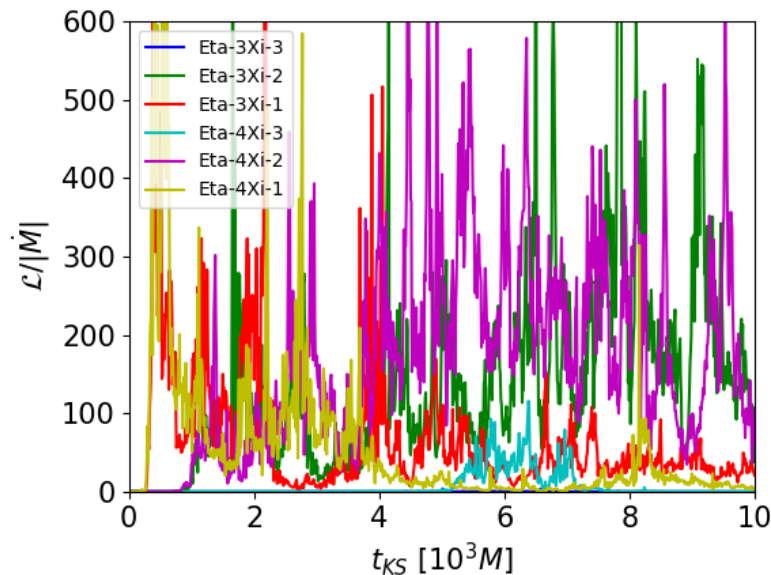


Figure 7. Time evolution of the pseudo-luminosity for each model. In runs with strong and intermediate dynamo, we see more noise than simulations of Porth and EHT-Collaboration [12].

4. Conclusions

We have discussed here an extension of our previous work, TO20, where the first GRMHD simulations of thick accretion disks with mean-field dynamo in a dynamic regime were presented. We have reproduced the SANE disk diagnostics of the Code Comparison Project of Porth and EHT-Collaboration [12] by expanding the range of resistivity and dynamo parameters compared to our previous paper. We have also extended the duration of simulations to investigate the stationary regime in more detail. Our main purpose is to show that the approach of mean-field dynamo in axisymmetric simulations is able to reproduce the amplification of the magnetic field due to MRI-driven turbulence. Even when starting from initial conditions not particularly favorable, such as a seed (toroidal) magnetic field with very low magnetization, our models can reproduce the same results of expensive 3D GRMHD simulations after saturation and dynamical quenching of the dynamo process.

We can summarize the results in the following points.

1. The action of a mean-field dynamo is able to generate equipartition-like poloidal fields as already seen in TO20 and later confirmed by Vourellis and Fendt [31].
2. In our simulations, we find a considerable dependence on the initialization value of the α effect. In particular, there is a minimum ξ_0 under which the dynamo is too weak to grow out the poloidal magnetic field significantly within the duration of our runs. On the other hand, an excessively high value causes a rapid and violent initial evolution, bringing a discrepancy of the diagnostics with the ideal three-dimensional case. However, we find an intermediate range that has a good agreement in all the diagnostics analyzed.
3. The dependence from η_0 is less evident in the horizon fluxes. However, the time averages in the stationary phase show that as η_0 increases, the average disk density decreases and the magnetization in the funnel increases. This is probably due to the

fact that the action of $\alpha\Omega$ dynamo is stronger, and it more effectively influences the accretion dynamics.

4. We evaluated the time evolution of the θ quality factor to test the ability to solve MRI in our simulations. In runs with intermediate and strong dynamo, the action of the dynamo combined with the adopted resolution allows for resolving the characteristic MRI wavelength during the initial phase. If the dynamo is too low, the instability can never develop. This behavior is confirmed by the fact that as ζ_0 increases, the accretion during the transient is progressively more intense. On the other hand, the stationary regime seems to be regulated exclusively by the action of the mean-field dynamo, as also stated by Vourellis and Fendt [31].

In conclusion, we believe that the much more computationally convenient approach of mean-field dynamo in axisymmetric simulations can reproduce SANE accretion disks whose properties are in accordance with the fully three-dimensional ideal simulations present in the literature. This result opens up the possibility of performing large parameter studies of axisymmetric thick disks to fit observational data and better constrain the physical properties of the accretion flows.

For the future, we aim to investigate the behavior of SANE disks for different profiles for the resistivity and mean-field dynamo coefficients [24] and to perform 3D simulations, so as to check whether our current results are robust, given that significant non-axisymmetric ideal and dynamo instabilities could arise [41]. Finally, we will extend our analysis to MAD disks, which will be the subject of the second part of the Code Comparison Project (Olivares et al. in prep).

Author Contributions: The authors contributed equally to this work. All authors have read and agreed to the published version of the manuscript.

Funding: MB acknowledges support from the European Research Council (ERC starting grant no. 715368—MagBURST).

Acknowledgments: The authors thank the three anonymous referees for their help in improving the manuscript. The authors gratefully acknowledge the Gauss Centre for Supercomputing e.V. (www.gauss-centre.eu) for funding this project by providing computing time on the GCS Supercomputer SuperMUC-NG at Leibniz Supercomputing Centre (www.lrz.de).

Conflicts of Interest: The authors declare no conflict of interest.

References

1. EHT-Collaboration. First M87 Event Horizon Telescope Results. V. Physical Origin of the Asymmetric Ring. *Astrophys. J.* **2019**, *875*, L5. [[CrossRef](#)]
2. EHT-Collaboration. First M87 Event Horizon Telescope Results. VIII. Magnetic Field Structure near The Event Horizon. *Astrophys. J. Lett.* **2021**, *910*, L13. [[CrossRef](#)]
3. Narayan, R.; Yi, I. Advection-dominated accretion: A self-similar solution. *Astrophys. J. Lett.* **1994**, *428*, L13–L16. [[CrossRef](#)]
4. Blandford, R.D.; Begelman, M.C. On the fate of gas accreting at a low rate on to a black hole. *Mon. Not. R. Astron. Soc.* **1999**, *303*, L1–L5. [[CrossRef](#)]
5. Narayan, R.; Igumenshchev, I.V.; Abramowicz, M.A. Self-similar Accretion Flows with Convection. *Astrophys. J.* **2000**, *539*, 798–808. [[CrossRef](#)]
6. Quataert, E.; Gruzinov, A. Convection-dominated Accretion Flows. *Astrophys. J.* **2000**, *539*, 809–814. [[CrossRef](#)]
7. Tchekhovskoy, A.; McKinney, J.C.; Narayan, R. General Relativistic Modeling of Magnetized Jets from Accreting Black Holes. *J. Phys. Conf. Ser.* **2012**, *372*, 012040. [[CrossRef](#)]
8. Igumenshchev, I.V.; Narayan, R.; Abramowicz, M.A. Three-dimensional Magnetohydrodynamic Simulations of Radiatively Inefficient Accretion Flows. *Astrophys. J.* **2003**, *592*, 1042–1059. [[CrossRef](#)]
9. Narayan, R.; Igumenshchev, I.V.; Abramowicz, M.A. Magnetically Arrested Disk: An Energetically Efficient Accretion Flow. *Publ. Astron. Soc. Jpn.* **2003**, *55*, L69–L72. [[CrossRef](#)]
10. Gammie, C.F.; McKinney, J.C.; Tóth, G. HARM: A Numerical Scheme for General Relativistic Magnetohydrodynamics. *Astrophys. J.* **2003**, *589*, 444–457. [[CrossRef](#)]
11. Narayan, R.; Sądowski, A.; Penna, R.F.; Kulkarni, A.K. GRMHD simulations of magnetized advection-dominated accretion on a non-spinning black hole: Role of outflows. *Mon. Not. R. Astron. Soc.* **2012**, *426*, 3241–3259. [[CrossRef](#)]

12. Porth, O.; EHT-Collaboration. The Event Horizon General Relativistic Magnetohydrodynamic Code Comparison Project. *Astrophys. J. Suppl. Ser.* **2019**, *243*, 26. [[CrossRef](#)]
13. Balbus, S.A.; Hawley, J.F. A powerful local shear instability in weakly magnetized disks. I—Linear analysis. II—Nonlinear evolution. *Astrophys. J.* **1991**, *376*, 214–233. [[CrossRef](#)]
14. Balbus, S.A.; Hawley, J.F. Instability, turbulence, and enhanced transport in accretion disks. *Rev. Mod. Phys.* **1998**, *70*, 1–53. [[CrossRef](#)]
15. Parker, E.N. Hydromagnetic Dynamo Models. *Astrophys. J.* **1955**, *122*, 293. [[CrossRef](#)]
16. Moffatt, H.K. *Magnetic Field Generation in Electrically Conducting Fluids*; Cambridge University Press: Cambridge, UK, 1978; 353p.
17. Krause, F.; Raedler, K.H. *Mean-Field Magnetohydrodynamics and Dynamo Theory*; Pergamon Press: Oxford, UK, 1980; 271p.
18. Schrunner, M.; Rädler, K.H.; Schmitt, D.; Rheinhardt, M.; Christensen, U.R. Mean-field concept and direct numerical simulations of rotating magnetoconvection and the geodynamo. *Geophys. Astrophys. Fluid Dyn.* **2007**, *101*, 81–116. [[CrossRef](#)]
19. Brandenburg, A.; Nordlund, A.; Stein, R.F.; Torkelsson, U. Dynamo-generated Turbulence and Large-Scale Magnetic Fields in a Keplerian Shear Flow. *Astrophys. J.* **1995**, *446*, 741. [[CrossRef](#)]
20. Ziegler, U.; Rüdiger, G. Shear rate dependence and the effect of resistivity in magneto-rotationally unstable, stratified disks. *Astron. Astrophys.* **2001**, *378*, 668–678.:20011245. [[CrossRef](#)]
21. Davis, S.W.; Stone, J.M.; Pessah, M.E. Sustained Magnetorotational Turbulence in Local Simulations of Stratified Disks with Zero Net Magnetic Flux. *Astrophys. J.* **2010**, *713*, 52–65. [[CrossRef](#)]
22. Hawley, J.F.; Guan, X.; Krolik, J.H. Assessing Quantitative Results in Accretion Simulations: From Local to Global. *Astrophys. J.* **2011**, *738*, 84. [[CrossRef](#)]
23. Hawley, J.F.; Richers, S.A.; Guan, X.; Krolik, J.H. Testing Convergence for Global Accretion Disks. *Astrophys. J.* **2013**, *772*, 102. [[CrossRef](#)]
24. Gressel, O.; Pessah, M.E. Characterizing the mean-field dynamo in turbulent accretion disks. *Astrophys. J.* **2015**, *810*, 59. [[CrossRef](#)]
25. Dhang, P.; Bendre, A.; Sharma, P.; Subramanian, K. Characterizing the dynamo in a radiatively inefficient accretion flow. *Mon. Not. R. Astron. Soc.* **2020**, *494*, 4854–4866. [[CrossRef](#)]
26. Bucciantini, N.; Del Zanna, L. A fully covariant mean-field dynamo closure for numerical 3 + 1 resistive GRMHD. *Mon. Not. R. Astron. Soc.* **2013**, *428*, 71. [[CrossRef](#)]
27. Del Zanna, L.; Bucciantini, N. Covariant and 3 + 1 equations for dynamo-chiral general relativistic magnetohydrodynamics. *Mon. Not. R. Astron. Soc.* **2018**, *479*, 657. [[CrossRef](#)]
28. Bugli, M.; Del Zanna, L.; Bucciantini, N. Mean Field Dynamo in Thick Disks around Kerr Black Holes: High Order Axisymmetric Simulations. *Int. J. Mod. Phys. Conf. Ser.* **2014**, *28*, 1460203. [[CrossRef](#)]
29. Franceschetti, K.; Del Zanna, L. General Relativistic Mean-field Dynamo Model for Proto-neutron Stars. *Universe* **2020**, *6*, 83. [[CrossRef](#)]
30. Tomei, N.; Del Zanna, L.; Bugli, M.; Bucciantini, N. General relativistic magnetohydrodynamic dynamo in thick accretion discs: Fully non-linear simulations. *Mon. Not. R. Astron. Soc.* **2020**, *491*, 2346–2359. [[CrossRef](#)]
31. Vourellis, C.; Fendt, C. Relativistic outflows from a GRMHD mean-field disk dynamo. *arXiv* **2021**, arXiv:2102.12482.
32. Vourellis, C.; Fendt, C.; Qian, Q.; Noble, S. GR-MHD disk winds and jets from black holes and resistive accretion disks. *Astrophys. J.* **2019**, *882*, 2. [[CrossRef](#)]
33. Mattia, G.; Fendt, C. Magnetohydrodynamic Accretion–Ejection: Jets Launched by a Nonisotropic Accretion-disk Dynamo. I. Validation and Application of Selected Dynamo Tensorial Components. *Astrophys. J.* **2020**, *900*, 59. [[CrossRef](#)]
34. Mattia, G.; Fendt, C. Magnetohydrodynamic Accretion–Ejection: Jets Launched by a Nonisotropic Accretion-disk Dynamo. II. A Dynamo Tensor Defined by the Disk Coriolis Number. *Astrophys. J.* **2020**, *900*, 60. [[CrossRef](#)]
35. Ripperda, B.; Bacchini, F.; Philippov, A.A. Magnetic Reconnection and Hot Spot Formation in Black Hole Accretion Disks. *Astrophys. J.* **2020**, *900*, 100. [[CrossRef](#)]
36. Fishbone, L.G.; Moncrief, V. Relativistic fluid disks in orbit around Kerr black holes. *Astrophys. J.* **1976**, *207*, 962–976. [[CrossRef](#)]
37. Del Zanna, L.; Zanotti, O.; Bucciantini, N.; Londrillo, P. ECHO: A Eulerian conservative high-order scheme for general relativistic magnetohydrodynamics and magnetodynamics. *Astron. Astrophys.* **2007**, *473*, 11.:20077093. [[CrossRef](#)]
38. Bugli, M. ECHO-3DHPC: Relativistic accretion disks onto black holes. *arXiv* **2018**, arXiv:1810.03542.
39. Bugli, M.; Iapichino, L.; Baruffa, F. ECHO-3DHPC: Advance the performance of astrophysics simulations with code modernization. *arXiv* **2018**, arXiv:1810.04597.
40. McKinney, J.C.; Tchekhovskoy, A.; Blandford, R.D. General Relativistic Magnetohydrodynamic Simulations of Magnetically Choked Accretion Flows around Black Holes. *Mon. Not. R. Astron. Soc.* **2012**, *423*, 3083–3117. [[CrossRef](#)]
41. Bugli, M.; Guilet, J.; Müller, E.; Del Zanna, L.; Bucciantini, N.; Montero, P.J. Papaloizou-Pringle instability suppression by the magnetorotational instability in relativistic accretion discs. *Mon. Not. R. Astron. Soc.* **2018**, *475*, 108. [[CrossRef](#)]